Bioactive heterobimetallic Re(I)/Au(I) complexes containing bidentate *N*-heterocyclic carbenes

Andrés Luengo,[†] Vanesa Fernández-Moreira,[†]* Isabel Marzo[‡] and M. Concepción Gimeno[†]*

[†]Departamento de Química Inorgánica, Instituto de Síntesis Química y Catálisis Homogénea (ISQCH), CSIC-Universidad de Zaragoza Pedro Cerbuna 12, 50009, Zaragoza, Spain

[‡]Departamento de Bioquímica y Biología Molecular, Universidad de Zaragoza, Pedro Cerbuna 12, 50009, Zaragoza, Spain.

Supporting Information Placeholder

ABSTRACT: The first cationic heterobimetallic complexes of the type *fac*-$[Re(CO)_3(NHC)(LAuPPh_3)]^+$, where NHC is an imidazole pyridine-based carbene and L is either 3-pyridylalkyne, 4-pyridylalkyne or 5-ethynyl-1-methyl-1*H*-imidazole, have been synthesized together with their Re(I) precursors. All of them have showed similar emissive properties resulting from the presence of the NHC system within the Re(I) core. Thus, emission can be ascribed as a phosphorescent process with a mixture of a MLCT from the Re(dπ) → NHC(π*), LLCT from the imidazolyl/pyridyl to the NHC ligand and LC (NHC derivative) transitions. In all cases, the emission maximum is blue shifted in comparison with that observed in the typical diimine-Re(I) systems. Only the heterobimetallic species displayed antiproliferative activity against tumor lung A549 cells, which was increased after irradiation at 405 nm up to nearly five times for complexes **4** and **5**. A necrotic process seems to be the preferred cell death mechanism. Fluorescence microscopy showed that only heterobimetallic complexes **4** and **5** were suitable for cell visualization. Their biodistribution pattern reveals accumulation within the cytoplasm close to the nucleus, and some nucleus permeation. Overall it can be suggested that whereas the emissive properties are dominated by the NHC-Re(I) fragment, the anticancer activity is mainly dependent on the Au(I) counterpart.

INTRODUCTION

Cancer is one of the diseases leading the causes of death in the last decade. For that reason, further research into new anticancer drugs is essential and one of the latest strategies to tackle this problem is to build bioactive trackable species.[1] The aim of this strategy is the compilation of information regarding the biodistribution and inner-interplay of drugs with the biological targets in order to design and deliver a sophisticated generation of anticancer metallodrugs. Within this frame several metallic structures combining well-known anticancer metal species such as Cisplatin,[2] Auranofin[3] or RAPTA[4] analogues with either an organic chromophore or an emissive metallic species have been already described, see Figure 1A. However, a step forward would be the incorporation of an emissive species that is able to add extra-antiproliferative value to the metalodrugs. Luminescent Re(I) complexes of the type *fac-*$[Re(N\text{^}N)(CO)_3(X/L)]^{+/0}$, where (N^N) represents a diimine derivative and X is a halogen or L a N-donor ligand, have been proven to be excellent cellular imaging agents for fluorescence microscopy.[5] Their emission is generally assigned to a ^{3}MLCT (metal-to-ligand-charge-transfer) transition, where the diimine is the main ligand contributor.[6] As consequence, L can be easily functionalized to introduce the bioactive fragment with no alterations of the emissive properties. In general, this type of Re(I) complexes do not seem to affect the antiproliferative properties when they are combined with a bioactive target (Figure 1B).[7] However, it was recently reported as the coordination of a bidentate *N*-heterocyclic carbene instead of the typical diimine ligand confers the Re(I) complex a remarkable anticancer activity against pancreatic cancer cells, see Figure 1B.[8] This was the first and the only example in which a Re(I) species containing a bidentate *N*-heterocyclic carbene has been tested as anticancer agent and based on the promising result it seems clear that the substitution of the typical diimine ligand for a bidentate NHC scaffold has been key to achieve an anticancer rhenium drug. Alternatively antimicrobial activity was also recently found for rhenium complexes containing monodentate NHC ligands.[9] Therefore, it can be postulated that combination of a NHC-Re(I) derivative with a metallodrug would be an excellent approach to maximise the therapeutic potential of a trackable metallodrug. Additionally, further substitution of L, which to the best of our knowledge has been only reported as a halogen for this type of Re(I) bidentate *N*-heterocyclic carbene derivatives[10] for a neutral N-donor ligand will deliver highly potential mitochondrial bioprobes as 1) cationic species present a greater predisposition to permeate those cellular membranes and 2) the N-donor ligand could be easily used as a linker to build the theranostic agents. Moreover, new grounds on the photophysical properties of these type of Re(I) complexes will be stablished. It is expected that their emissive behavior will differ from that seen for the reported neutral NHC-Re(I) complexes studied.[11]

Thus, herein we describe the first approach towards the use of luminescent *N*-heterocyclic carbene based-Re(I) species as cell imaging agents as well as building blocks for trackable anticancer metallodrugs.

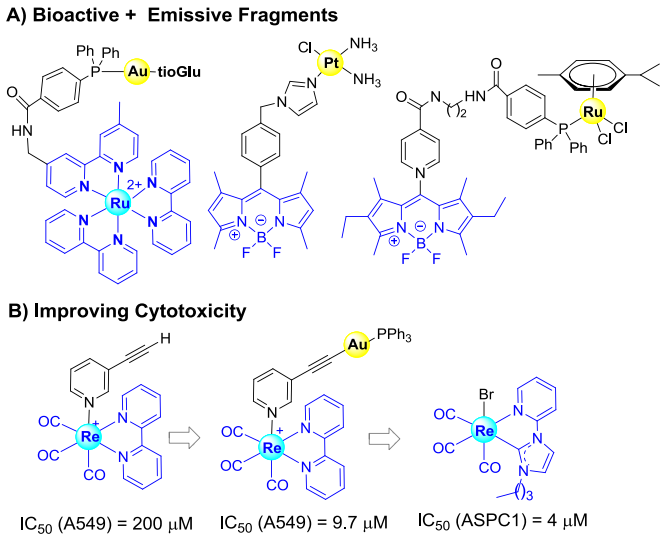

Figure 1. A) Examples of the combination of bioactive and emissive fragments; B) Examples of cytotoxicity displayed by either diimine or NHC-Re(I) derivatives.

RESULT AND DISCUSSION

Synthetic Approach. In previous studies we have validated the possibility of visualizing bioactive gold(I) complexes in cancer cells by combination of the bioactive metallic fragment with a luminescent Re(I) species, using either functionalized alkynes or phosphines as linkers.[7] In the present work the focus is set on the development of lumininescent heterobimetallic Re(I)/Au(I) complexes with an improved antiproliferative activity towards cancer cells. For that, substitution of the typical diimine ligand within the Re(I) scaffold by an analogous *N*-heteroclyclic carbene (NHC) chelate is proposed. These systems would deliver the first example of a NHC-Re(I)/Au(I) heterobimetallic complex used for cellular imaging and as anticancer agent. Similarly to previous synthetic procedures the *N*-methyl-*N*'-2-pyridylimidazolium salt was prepared by nucleophilic substitution of imidazole with 2-bromo-pyridine followed by an imidazole alkylation reaction with methyl iodide.[12] The *N*-methyl-*N*'-2-pyridylimidazolium salt reacts with silver oxide forming the silver carbene that in situ transmetalates with $Re(CO)_5Cl$, in acetonitrile, to give **A** in a moderate yield.[13] It is worth noticing the presence of the chelated NHC within the *fac*-{$Re(I)CO_3$} core instead of the symmetric diimine ligand generate a pair of enantioners. Therefore, further modification of **A** leads to subsequent racemic mixtures. Afterwards, abstraction of the chloride ligand by silver triflate in acetonitrile led to an activated Re(I)-NHC species **B**, which can be easily derivatized by further substitution of the labile acetonitrile ligand for the corresponding alkyne derivatives to obtain complexes **1-3**. In order to prepare the bimetallic Re(I)/Au(I) species, the Re(I) precursor was stirred in either DCM or acetonitrile in the presence of $Au(acac)PPh_3$. The acetylacetonate complex facilitates the deprotonation of the alkyne and the subsequent coordination of the gold atom to the triple bond, thus affording the bimetallic complexes **4-6**. All complexes have been characterized by ^1H, $^{13}C\{^1H\}$, $^{31}P\{^1H\}$ NMR, FT-IR, UV-Vis spectroscopy as well as mass spectrometry corroborating the accomplishment on their synthesis. Analysis of the CO stretching frequencies of all the complexes corroborate the expected facial arrangements as three stretches at c.a. 2020, 1940 and ca. 1890 cm^{-1} for complexes **1-3** and two stretches for **4-6** around 2022, 1900 cm^{-1} are observed because of the overlap of A'(2) and A'' modes into a single broad band. Similar NHC-rhenium tricarbonyl derivatives presented analogous values.[14] Moreover, the heterobimetallic complexes lack of υ(H-C≡C) band, which had been observed for their Re(I) precursors, indicating the coordination of the gold fragment, see Table 1. Additionally, in all cases, ^1H-NMR spectra were well defined and showed the typical patterns for the *N*-methyl-*N*'-2-pyridylimidazolium and the correspondent pyridyl or imidazolyl carbene derivative coordinated to a *fac*-$Re(CO)_3$ core. Specifically, it was observed the disappearance of the acidic imidazolium proton signal in the 10-12 ppm region of the ^1H-NMR spectrum. Consequently, a new carbenoic carbon signal appears between 189 and 197 ppm in the ^{13}C NMR spectra together with the carbonyl carbons, confirming the coordination of NHC as a bidentate ligand to the rhenium core.[15] Moreover, as a result of the gold triphenylphosphine coordination, the heterobimetallic complexes (**4-6**) revealed in their ^1H-NMR spectra a new multiplet resonance in the region between 7.49 and 7.55 ppm due to the presence of the new fragment, as well as the disappearance of the terminal alkyne protons present in their precursors at 3.70, 3.62 and 3.50 ppm respectively, in concordance with the IR results. On top of that, the downfield shift of the alkynyl carbons seen by ^{13}C-NMR spectroscopy upon the coordination of -$AuPPh_3$ and the single peak c.a. 41 ppm observed by ^{31}P NMR spectroscopy is consistent with those values obtained for similar species.[7a] Further analytical data provided by mass spectrometry corroborated the accomplishment on the synthesis.

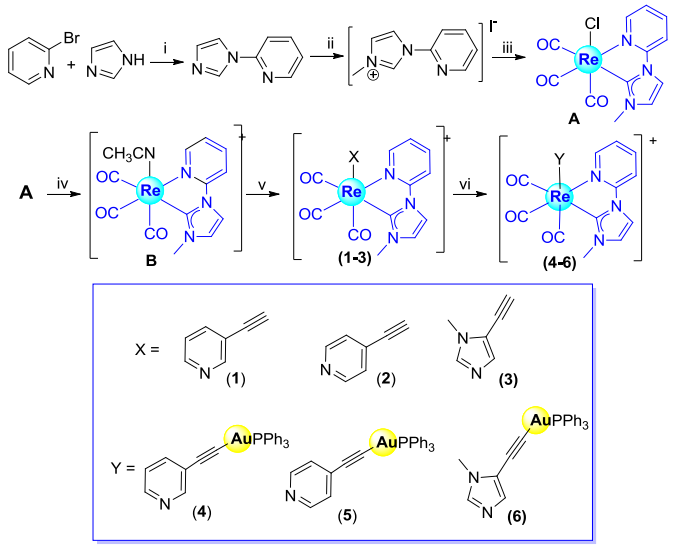

Figure 2. Schematic synthetic procedure and depiction of final complexes (**1-6**). i) K_2CO_3, 190 ºC, 18 h; ii) MeI, THF, rt, 24 h; iii) Ag_2O, $Re(CO)_5Cl$, CH_3CN; iv) AgOTf, CH_3CN, reflux 5 h; v) alkynylpyridine derivative, THF, reflux; vi) $Au(acac)PPh_3$, DCM.

Table 1. IR Stretching bands (cm^{-1}) and $^{31}P\{^1H\}$ and $^{13}C\{^1H\}$ NMR (ppm) chemical shifts (CD_2Cl_2) of **1–6**.

	IR(υ(CO))	IR(υ (H-C≡C))	$^{31}P\{^1H\}$-NMR	^{13}C-NMR(*C*≡C-

				H/Au)
1	2022s, 1926m, 1895s	3238w	-	78.0[a]
2	2019s, 1955m,1908s	3236w	-	79.5
3	2023s, 1945m,1887s	3229w	-	69.2
4	2023s, 1900s,br	-	41.5	98.0
5	2021s, 1897br	-	41.5	99.2
6	2019s, 1893br	-	41.8	no

w: weak, m: medium, s: strong, br: broad, a (CD_3CN). no: Not Observable.

Crystal Structures. Complexes **B**, **1**, **3** are chiral complexes and have been crystalized as racemic mixtures by slow diffusion of Et_2O in CH_2Cl_2 (**1**, **3**) or CH_3CN (**B**). Molecular structures together with selected bond distances and angles are presented in Table 2 and Figure 3. The three complexes presented a single molecule per asymmetric unit and their space groups are Pn, $P2_1/n$ or $P2_1/c$, respectively. On the contrary, the enantiomers of all the species can be observed in the packing of the species, see Figure S1. In all cases, the rhenium coordination sphere could be described as a distorted octahedron, where the three carbonyls are arranged in a facial disposition. Thus, the NHC system lies on the equatorial plane together with two carbonyl ligands, whereas the remaining carbonyl and the correspondent N-donor ligand are located in the axial positions of the octahedron. The Re-$C_{carbene}$ distances are 2.125(5), 2.130(4), 2.135(6) Å for complexes **B**, 1 and **3** respectively, which are very close values to those reported for similar carbene Re species.[16] Moreover, bond distances of Re-CO *trans* to the NHC unit were much longer (c.a. 1.970 Å) in comparison with that of the other Re-CO distances (c.a. 1.915 Å) due to the well-known *trans* influence of NHCs species. Consequently, it was observed a shortening of the C-O bond length of the correspondent carbonyl *trans* to the NHC as a result of the lower π back-bonding character from the metal to the carbonyl unit, see caption in Figure 3. These bond length differences are in agreement with the published crystallographic data of similar NHC-rhenium complexes.[11b] It is also worth mentioning that the NHC chelate provides a similar constriction to the complex than their analogues bipy[17] or phen[18] chelates, with narrow C-Re-N angles at c.a. 74°, comparable to those of the cited bidentate ligands.

Table 2. The most relevant bond lengths (Å) and angles (°) of Complex **B**, Complex **1** and Complex **3**.

Complex B	**Complex 1**	**Complex 3**
Re(1)-C(1): 1.911(5)	Re(1)-C(1): 1.968(4)	Re(1)-C(1): 1.921(4)
Re(1)-C(2):1.972(6)	Re(1)-C(2): 1.911(4)	Re(1)-C(2): 1.968(6)
Re(1)-C(3): 1.906(6)	Re(1)-C(3): 1.935(4)	Re(1)-C(3): 1.906(4)
Re(1)-C(4): 2.125(5)	Re(1)-C(9): 2.130(4)	Re(1)-C(4): 2.135(6)
Re(1)-N(3): 2.202(4),	Re(1)-N(1): 2.212(3)	Re(1)-N(3): 2.192(4)
Re(1)-N(4): 2.144(5)	Re(1)-N(4): 2.225(3)	Re(1)-N(4): 2.188(3)
C(1)-O(1): 1.156(6)	C(1)-O(1): 1.144(4)	C(1)-O(1): 1.141(5),
C(2)-O(2): 1.140(7)	C(2)-O(2): 1.149(5)	C(2)-O(2): 1.146(7),
C(3)-O(3): 1.1569(7),	C(3)-O(3): 1.149(5)	C(3)-O(3): 1.155(6)
N(4)-Re(1)-C(3): 175.7(3)	N(4)-Re(1)-C(3): 178.7(1)	N(4)-Re(1)-C(3): 174.3(2),
C(4)-Re(1)-N(3): 74.6(2)	C(9)-Re(1)-N(1): 74.5(1)	C(9)-Re(1)-N(3): 74.9(2)

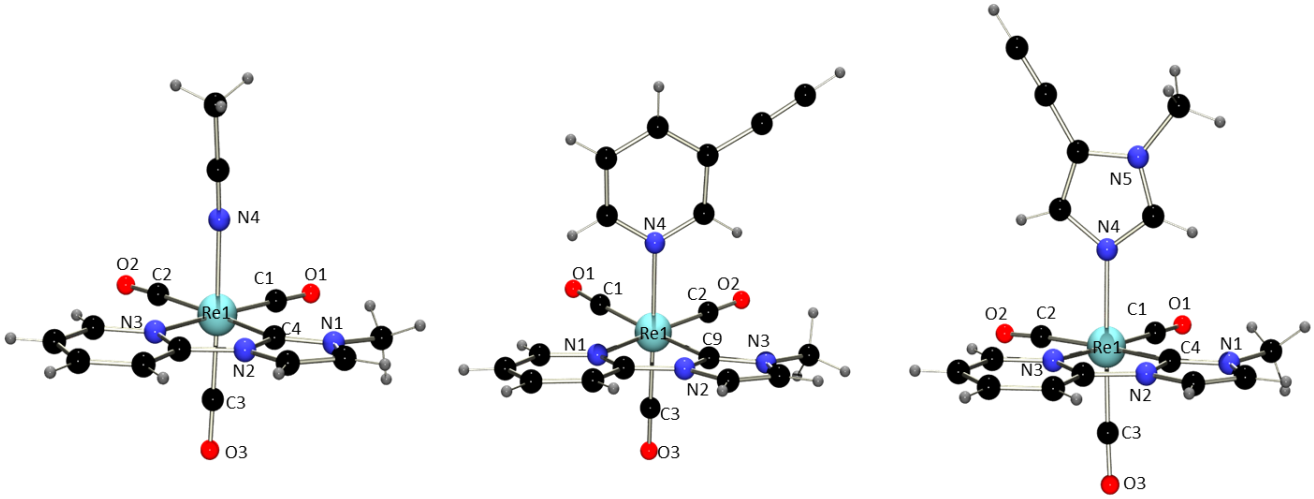

Figure 3. Pov-ray representation of complexes **B**, **1** and **3** (the triflate counter ions were omitted for clarity). Note that all the selected species are of the same chirality.

Optical Properties. The photophysical properties of complexes **1**-**6** were analyzed by UV-Vis absorption and emission spectroscopy in dimethyl sulfoxide solution at room temperature. The most significant data are collected in Table 3 and Figures 4 and S2-S3. All the complexes showed a similar absorption pattern, with an intense absorption band at c.a. 290 nm that can be attributed to $\pi\rightarrow\pi^*$ transitions within the NHC ligand and also within the phenyl groups in the case of the heterobimetallic complexes. Additionally, all of them presented a lower energy band of relatively small molar absorptivity above 300 nm. This band could be attributed to a mixture of MLCT (Re→NHC) and LLCT (pyridyl/imidazolyl→NHC) charge transfer transitions, and thus, it is best described as a MLLCT.[13,14] Regarding the emissive properties, these complexes presented blue shifted emission maxima in comparison with those of the typical $[Re(CO)_3(N\text{^}N)L]^{0/+}$.[6] Such blue shift is result of the strongly σ-donating NHC ligands, which ensures strong ligand fields with high lying d–d excited states. Specifically complexes **1**, **2**, **4** and **5** exhibit a structured emission at c.a. 481 nm, whereas complexes **3** and **6** presented a slightly red shifted broad emission band at 488 and 490 nm, respectively, see Figures 4 and S3. The fact that the imidazolyl derivatives **3** and **6** presented emission maxima red shifted in comparison with their analogues **1**, **2**, **4** and **5** species could be associated to the higher electron donating character of the imidazole vs pyridyl derivative present in axial position of the Re(I) metal center. In consequence, the HOMO orbitals, which are primary located in the Re(I), get slightly destabilized and a red shift on the emission maximum is seen.[15a] The emissions could be therefore attributed to a MLLCT transition, i.e. a MLCT from the Re(dπ)→NHC(π*) mixed with a LLCT transitions from the imidazolyl/pyridyl to the NHC ligand. On top of that, it is also worth mentioning that the structured emission profile observed especially for complexes **1**, **2** and **4** and **5** suggest that the MLLCT could be partially mixed with a ^{3}LC state.[13] Demas and DeGraff already postulated such behavior in the cases where MLLCT and LC states were energetically similar.[19] The significant LC state contribution to the emission was also deducible from the similarities between the excitation and emission profile of the imidazolium salt itself with that of the complexes, see Fig S3. Lifetime values at room temperature ranges from tens to hundreds of nanoseconds, which are typical of phosphorescent nature in this family of complexes.[15] Additionally, the presence of the gold fragment grafted in the axial ligand does not seem to affect the photophysical behavior of the species, which is in concordance with other heterobimetallic species reported.[7a]

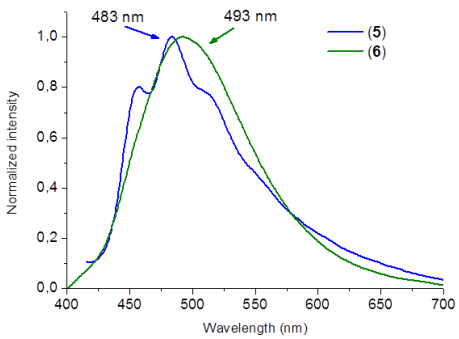

Figure 4. Emission spectra of complexes **5** and **6** in degassed DMSO at 298 K.

Table 3. Photophysical properties of **1**-**6** in degassed DMSO solution.

	λ_{abs}/nm (ε / L×mol^{-1}×cm^{-1})	λ_{em}/nm (λ_{em}/nm)	τ / ns
1	288 (14000), 320 (8000)	440, 460(s) (400)	-
2	291 (14800), 317 (10900)	456, 481(s), 514 (413)	212
3	286 (10100), 323 (5800)	488 (370)	10, 136
4	285 (36700), 316 (14600)	460, 485(s), 514 (414)	31, 205
5	288 (30300), 310 (28170)	465, 483(s), 512 (412)	207
6	280 (25400), 339 (4000)	493(377)	15, 123

Aerated DMSO: τ(**2**) = 175 ns. Degassed DMSO **Imidazolium salt**: λ_{em}= 440 nm (λ_{exc} 295 nm); **A** λ_{em}= 506 nm (λ_{exc} 401 nm) (s) strong

Biological Properties. The cytotoxic activity of complexes **1** to **6** as well as their rhenium precursors **A** and **B** was determined by an MTT assay in the tumor lung A549 cell line, see Table 4. Only the heterobimetallic complexes presented a significant antiproliferative character, c.a. 11 μM. On the contrary, the monometallic rhenium complexes showed in all cases cytotoxicity values over 50 μM, which point towards the gold fragment as the bioactive entity for complexes **4**-**6**. As similar NHC rhenium derivatives have been proven to dissociate CO under photochemical conditions,[15b] complexes **A**, **B** and **1** to **3** were tested as photocytotoxic agents using the same cell line. However, irradiation at 405 nm for 10 minutes did not showed the expected increase of toxicity. Once again all of them presented IC_{50} values over 50 μM. In addition to the monometallic species, the heterobimetallic complexes were also analyzed under photochemical conditions. All of them showed a slightly improvement of their antiproliferative character, see Table 4, being complex **6** the less affected by the application of the irradiation. Despite the promising result, these complexes could not be considered as effective photocytotoxic agents as their level of toxicity in absence of light is already high (c.a. 11 μM). Cell death mechanism of heterobimetallic complexes was investigated by flow cytometry, see Fig. S4. Complex **4** was incubated at different concentrations with A549 cells for 24 h. Annexin V-DY634 and 7-AAD were used as fluorescent markers. Annexin V-DY634 binds to phosphatidylserine in the cell membrane and 7-AAD is a vital dye that only enters through damaged cell membrane. Moreover, Z-VAD-fmk, a cell permeant pan caspase inhibitor, was used as an indicator of the participation of caspases in the cell death. Since the cells incubated with both markers seemed to have a positive response by flow cytometry together with the speed of cell death observed, it can be concluded that the cell death mechanism is likely to be by a necrotic process. Moreover, the fact that the cells incubated with Z-VAD-fmk behave in the same way that the ones lacking of such caspase inhibitor corroborates that the cellular death is following a pathway independent of caspases, see Figure S5. Additionally, a similar

experiment was performed but this time irradiating the samples for ten minutes at 405 nm during the incubation period in order to assess whether the irradiation process was affecting the cellular death pathway somehow. Once again the result was similar to the non-irradiated experiment; a necrosis seems to be the preferred cellular death. Investigations regarding the biological targets for these complexes were also undertaken. Thus, inhibition of the thioredoxin reductase was performed using complex **4** as model. Specifically, A549 cells were treated with complex **4** or vehicle (DMSO) for 4 h. Then, total protein extracts were prepared and used for the determination of thioredoxin activity. Thereafter, the artificial substrate 5,5'-dithiobis-(2-nitrobenzoic acid) (DTNB) was added, which would rapidly evolve to two molecules of 2-nitro-5-thiobenzoaye anion (TNB) if thioredoxin redutase is in the presence of NADPH. The reduction of DTNB to TNB affords a yellow color that can be detected at 412 nm by UV-Vis absorption.[20] The evolution of the TNB formation was recorded for 5 min and its comparison with that of a control assay did not show inhibition of the thioredoxin, see figure 5. This result was further confirmed by a preliminary analysis on the production of reactive oxygen species (ROS) in colorectal adenocarcinoma cells (CACO cells). Once again, incubation of complex **4** with CACO cells did not promote the production of ROS, which suggest a different biological target than that of thioredoxin.

Table 4. IC_{50} values of **1**-**6** in A549 cells after incubation for 24 h in absence of light and after irradiation for 10 min at 405 nm.

	IC_{50}	IC_{50}**(irradiated)**
1	>50	>50
2	>50	>50
3	>50	>50
4	12.18 ± 1.19	4.48 ± 0.71
5	10.82 ± 1.63	2.66 ± 0.56
6	12.65 ± 2.10	9.97 ± 3.04
A	>50	>50
NHC	>50	>50

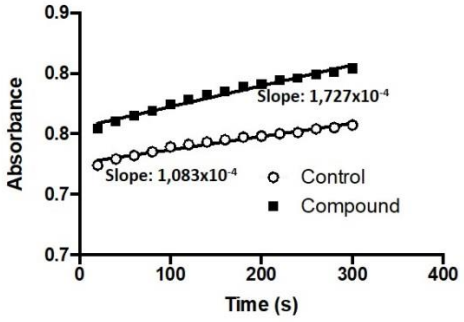

Figure 5. Inhibition of thioredoxin assay for complex **4**. Representation of the evolution of absorbance intensity of TNB during 5 minutes.

In an attempt to elucidate the biodistribution of the complexes **1**-**6**, fluorescence microscopy was used. The species were incubated with A549 cells for 24 h at a concentration lower than their IC_{50} value in order to prevent cell death during the experiment. In addition to them, Draq5, a nuclear dye with an excitation wavelength of 647 nm, was used as internal standard to ascertain their localization. Cellular images were taken after exciting the cells at 405 nm, where the emissive complexes could be visualized. Superimposition of those with the correspondent images taken after exciting the samples at 647 nm, allowed elucidating whether the complexes **1**-**6** were within the cell and/or inside the nucleus. Unexpectedly, none of the monometallic rhenium complexes were visible within this assay. In contrast, two out of the three heterobimetallic complexes showed emission within the cytoplasm surrounding of the nucleus, and in a smaller amount inside the nucleus, Figure 6 and 7. Specifically, **4** and **5** were the complexes that were able to be visualized within the cell. A closer look to other heterobimetallic Re(I)/Au(I) complexes reported in the literature as possible cell visualization or theranostic agents indicates that typically those containing in their structure the fragment $AuPPh_3$ appear to have more permeability than their rhenium monometallic analogues.[7] The present case seems to follow the same trend except for complex **6**, which despite having a $–AuPPh_3$ fragment was not observable. A plausible explanation for this result might relay on the photophysical properties of complex **6**. Contrary to complexes **4** and **5**, whose maximum excitation wavelengths were laying around 410 nm in both cases, in complex **6** the maximum excitation was at 377 nm, see Table 3 and Fig. S3. Therefore, irradiation of the cells at 405 nm would not be suitable to excite complex **6**, and in consequence emission will not be observed. This result goes in line with the lower photocytotoxicity seen in the case of complex **6** in comparison with complexes **4** and **5**, see Table 4. It is possible that the irradiation used is no equally effective.

As previously commented, complexes **1**-**3** were neither suitable for cell imaging within these conditions. To assess whether a possible disruption of the molecules under biological conditions was taking place and thus, preventing their visualization, a stability assay was performed. Specifically, complexes **1** and **4** were chosen as representative species and they were dissolved in a mixture of DMSO:PBS (< 0.5% DMSO). Stability of the complexes was analyzed by UV-Vis absorption spectroscopy over a period of 24 h. Both of them seem to remain stable under those conditions, see Figure S6. Therefore, it seems clear that decomposition of the complexes could not be the origin of the lack of response in the localization experiment for the monometallic species **1**-**3**. The main difference between these Re(I) species and the ones already studied by fluorescence microscopy is the nature of the chelated ligand.[21] Thus, changing the typical diimine ligand for a pyridyl-carbene derivative (NHC) seems to negatively affect the internalization process.

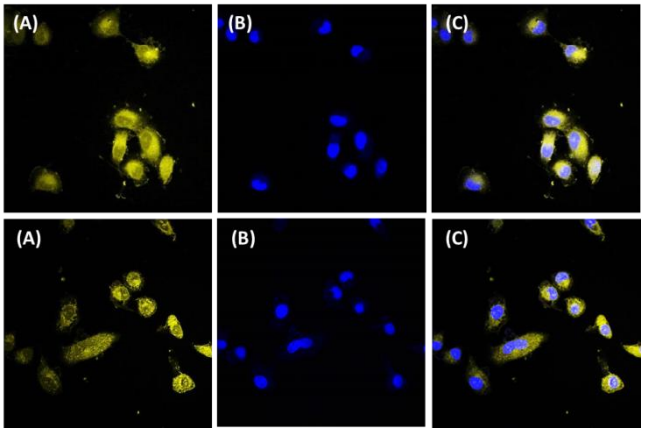

Figure 6. Images of complexes **4** (top row) and **5** (bottom row) incubated with A459 cells and Draq5 at 37 C for 4 h. (A) After irradiation at 405 nm. (B) After irradiation at 647 nm. (C) Superimposition image.

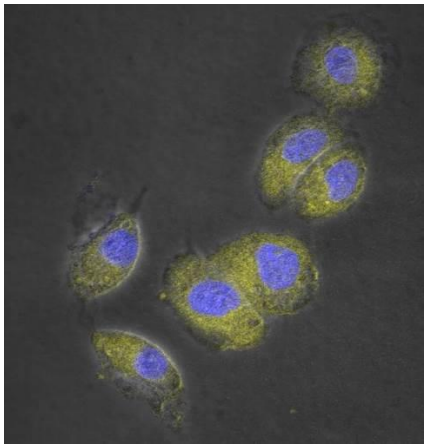

Figure 7. Image of complexes **5** (yellow color) incubated with A459 cells and Draq5 (blue color) at 37 C for 4 h superimposed with the bright field image.

CONCLUSIONS

In summary, the first bioactive and luminescent heterobimetallic Re(I)/Au(I) complexes containing a pyridyl *N*-heterocyclic carbene derivative instead of the typical diimine ligand were reported, as well as their monometallic Re(I) precursors. Either pyridyl or imidazolyl alkyne derivatives were used as bridge ligand between both metals, being specifically bounded to the Re(I) center through the nitrogen atom and to the Au(I) center through the alkynyl carbon. The photophysical properties of these complexes showed that all of them have a similar behavior, where the presence of the Au(I) fragment was not implicated in the emissive process. Thus, the emission was attributed to a mixture of ^{3}MLCT from the Re(dπ) → NHC(π*), ^{3}LLCT from the imidazolyl/pyridyl to the NHC ligand as well as ^{3}LC (NHC derivative) transitions. The similar structured emission profile seen for NHC, **1**, **2**, **4**, **5** was conclusive on the implication of LC transitions. Moreover, such LC contribution seems to be less marked in the case of complexes with axial ligands like a chloride (A) or imidazolyl derivatives (**3** and **6**), whose electron donating character is higher, and presumably the contribution of the LLCT over the LC transition too. As expected, only the heterobimetallic complexes showed antiproliferative character against A549 cells ($IC_{50} \approx 11$ μM). Therefore, at this point it can be stated that we have developed heterobimetallic species able to combine their intrinsic emissive (Re(I) fragment) and bioactive (Au(I) fragment) properties into a new single molecular structure. Additionally, irradiation of the cells incubated with the heterobimetallic complexes at 405 nm incremented the cytotoxicity up to five times in some cases. In contrast, monometallic Re(I) species did not show any extra antiproliferative activity. The cell death mechanism studied by flow cytometry concluded that a necrotic process seems to take place for the irradiated and no-irradiated assay. Moreover, fluorescence microscopy analysis showed that only **4** and **5** were able to accumulate within the cells. Specifically, their emission was within the cytoplasm surrounding of the nucleus, and in a smallest amount inside the nucleus. The fact that none of the monometallic Re complexes were detected by this technique could be a combination of several factors. Both photophysical (lower intensity or quenching processes in the biological media) and/or the different lipophilic properties (lack of the gold triphenyl fragment and the presence of pyridyl-NHC derivative instead of the typical diimine) could be implicated. Additionally, the different photophysical properties seem to be the origin for not being able to detect **6** by fluorescence microscopy. In this particular case we believe that it is possible that the complexes have entered the cells as it is known that the fragment $AuPPh_3$ renders a higher lipophilicity of the probe and thus, a better cell permeability. However, this complex has a maximum excitation wavelength of c.a. 370 nm, which is quite far away from the excitation wavelength used within the visualization experiment (405 nm).

To conclude, the development of heterobimetallic Re(I)/Au(I) complexes as emissive and bioactive species could be achieved attending to the different functionalization of a) the chelate ligand NHC to modulate the desired photophysical properties and b) the bridging and ancillary gold ligand in order to endow specific bioactivity.

EXPERIMENTAL SECTION

General Measurements and Analysis Instrumentation. Mass spectra were recorded on a BRUKER ESQUIRE 3000 PLUS, with the electrospray (ESI) technique and on a BRUKER (MALDI-TOF). ^{1}H, ^{13}C{^{1}H} and ^{31}P{^{1}H} NMR, including 2D experiments, were recorded at room temperature on a BRUKER AVANCE 400 spectrometer (^{1}H, 400 MHz, ^{13}C, 100.6 MHz, ^{31}P, 162 MHz) with chemical shifts (δ, ppm) reported relative to the solvent peaks of the deuterated solvent. Infrared spectra were recorded in the range 4000–250 cm^{-1} on a Perkin-Elmer Spectrum 100 FTIR spectrometer. Room temperature steady-state emission and excitation spectra were recorded with a Jobin-Yvon-Horiba fluorolog FL3-11 spectrometer fitted with a JY TBX picosecond detection module. Nanosecond lifetimes were recorded with a Datastation HUB-B with a nanoLED controller and software DAS6. The nanoLEDs employed for lifetime measurements were of 370 and 390 nm. The lifetime data were fitted using the Jobin-Yvon software package and the Origin Pro 8 program. UV-Vis

spectra were recorded with a 1 cm quartz cells on an Evolution 600 spectrophotometer. The quantum yields were measured in a Hamamatsu Photonics Quantaurus-QY 300-950 nm.

Crystal Structure Determinations. Crystals were mounted in inert oil on glass fibers and transferred to the cold gas stream of an Xcalibur Oxford Diffraction diffractometer equipped with a low-temperature attachment. Data were collected using monochromated MoKα radiation (λ= 0.71073 Å). Scan type ω. Absorption correction based on multiple scans were applied using spherical harmonics implemented in SCALE3 ABSPACK scaling algorithm. The structures were solved by direct methods and refined on F^2 using the program SHELXL-97.[22]All non-hydrogen atoms were refined anisotropically, with the exception of complex **7**. CCDC deposition numbers 1858777 (**B**) 185878 (**1**) and 1858779 (**3**) contain the supplementary crystallographic data. These data can be obtained free of charge by The Cambridge Crystallography Data Center.

Antiproliferative studies: MTT assay. Exponentially growing cells (A549) were seeded at a density of approximately 10^4 cells per well in 96-well flat-bottomed microplates and allowed to attach for 24 h prior to addition of compounds. The complexes were dissolved in DMSO and added to cells in concentrations ranging from 10 to 200 μM in quadruplicate. Cells were incubated with our compounds for 24 h at 37 °C. Ten microliters of MTT (5 mg ml^{-1}) were added to each well and plates were incubated for 2 h at 37 °C. Finally, the growth media was eliminated and DMSO (100 μl per well) was added to dissolve the formazan precipitates. The optical density was measured at 550 nm using a 96-well multiscanner autoreader (ELISA). The IC_{50} was calculated by nonlinear regression analysis.

Flow cytometry assay. The cells were treated for 24 h with compound **4** at 5, 10 and 25 μM. Then, they were trypsinised and incubated at 37 °C for 5 minutes in ABB (140 mM NaCl, 2.5 mM CaCl2, 10 mM Hepes/NaOH, pH 7.4) containing 0.5 mg ml^{-1} of either annexin V-DY634 or 7-AAD. Finally, the cells were diluted to 0.5 ml with ABB and analysed by flow cytometry (FACScan, BD Biosciences, Spain).

Thioredoxin inhibition assay. For determination of the thioredoxin reductase activity, A549 cells were incubated for 9 h with our compound at different concentrations near IC50 values. Cells were collected and washed with PBS and 150 μl buffer (1% Triton X-100, 150 mM NaCl, 50 mM Tris/HCl pH 7.6, 10% v/v glycerol, 1 mM EDTA, 1 mM sodium orthovanadate, 10 mM sodium pyrophosphate, 10 μg ml^{-1} leupeptin, 10 mM NaF, 1 mM sodium methylsulphonium) for 30 min at 0 °C, and centrifuged at 200 g for 10 min at 4 °C. The protein was quantified using the BCA protein assay (Thermo Scientific) and 80 μg was added in each assay. Kinetic studies were performed in a buffer containing 0.2 M NaCl, H-phosphate pH 7.4, 2 mM EDTA, 0.25 mM NADPH and 3 mM DTNB. The increase in the absorbance was measured at 412 nm for 5 min at 25 °C.

Intracellular peroxides (ROS) formation. The production of ROS (Reactive Oxygen Species) was assessed using the dichlorofluorescein (DCF) assay.[23] Caco-2/TC7 cells were plated in 96-well plates at a density of 4000 cells perwell and incubated for 24 h under standard cell culture conditions. For treatment, **4** was added to cells within its IC_{50} concentration that of IC_{50} and incubated 24 h; mock treated cells were just incubated with DMSO at the same concentration than treated cells. Then, cells were washed twice with PBS and 100 μL of 20 mM DCFH-DA (dichloro-dihydrofluoresceindiacetate) were added to each well. Cells were incubated 1 h at 37 °C and washed twice with PBS; finally, 100 μL of PBS were added and fluorescence was analyzed with DTX-880 (Beckman Counter). Excitation and emission settings were 485 and 535 nm, respectively. The intensity of fluorescence is considered as a reflection of total intracellular ROS.

Cell fluorescence microscopy study. European Collection of Cell Cultures, were maintained in Hepes modified minimum essential medium (DMEM) supplemented with 5% fetal bovine serum, penicillin, and streptomycin. A549 cells were detached from the plastic flask using trypsin-EDTA solution and suspended in an excess volume of growth medium. The homogeneous cell suspension was then distributed into 24-well flat-bottomed microplates over a cover slip placed inside each well and they were allowed to attach for 24 h prior to addition of compounds. Complexes were added (10 μl) to the cells up to a final concentration of 25 μM. After incubation for 4 h at 37 °C, the growth medium was removed and 0.5 ml of PBS was added for a washing step (3 times). Thereafter, 0.5 ml of paraformaldehyde (4%) was added and allowed to stand for 15 min at room temperature. Eventually the paraformaldehyde was removed and further washings with PBS were performed (3 × 0.5 ml). The cover slips were collected from the 24 well plate, immersed for 1 or 2 seconds in distilled water and let them to drip the water. Then, they are placed over a microscope slide where a drop of fluoromount with 2 μM DRAQ5 was previously placed. Preparations were viewed using an Olympus FV10-i Oil type compact confocal laser microscope using a ×10 or ×60 objective, with excitation wavelength at 405 and 650 nm.

Materials and Procedures. The starting material *N*-methyl-*N*'-2-pyridylimidazolium,[12] Au(acac)(PPh_3)[24] and complex **A**[13] were prepared according to literature procedures and their experimental data agrees with that reported somewhere else. All other starting materials and solvents were purchased from commercial suppliers and used as received unless otherwise stated.

Synthesis of complex B. To a stirred solution of **A** (83 mg, 0.178 mmol) in CH_3CN (20 mL) was added AgOTf (50.4 mg, 0.196 mmol) and refluxed over 5 h and 30 minutes in the dark. The suspension was filtered over celite and the solvent reduced to minimum volume. The addition of cold ether afforded an oil which was to afford the product as a pale yellow solid. (83 mg, 79 %). ^{1}H NMR (400 MHz, CD_2Cl_2) δ 8.76 (ddd, *J* = 5.6, 1.6, 0.7 Hz, 1H, H_6), 8.25 (ddd, *J* = 8.4, 7.6, 1.6 Hz, 1H, H_4), 8.14 (d, *J* = 2.2 Hz, 1H, H_8 or H_9), 8.13 – 8.10 (ddd, *J* = 8.4, 1.2, 0.7 Hz, 1H, H_3), 7.44 (ddd, *J* = 7.5, 5.6, 1.2 Hz, 1H, H_5), 7.29 (d, *J* = 2.2 Hz, 1H, H_8 or H_9).^{13}C NMR (101 MHz, CD_2Cl_2) δ 195.0 (s, CO), 194.7 (s, CO), 189.2 (s, CO), 187.0 (s, C_7), 154.3 (s, C_2), 153.8 (s, C_6), 143.7 (s, C_4), 125.8 (s, C_8 or C_9), 124.8 (s, C_5), 118.90 (s, C_8 or C_9), 114.32 (s, C_3), 39.78 (s, C_{10}), 4.32 (s, C_{12}). HRMS (m/z): 471.0470 [M-OTf], $C_{14}H_{12}N_4O_3Re$ (471.0462). IR (cm^{-1}): υ 3155 (C_{Ar}-H), υ 2027, 1882 (CO), υ 1621 (C_{Ar}=N)

General procedure for coordination synthesis of 1-3. To a stirred solution of **B** in THF was added the corresponding alkynylpyridine ligand and the reaction mixture was heated several hours until consumption of the starting material. The solvent was then evaporated and the crude mixture redissolved in DCM. Filtration over celite followed by addition of ether afforded the desired product as a pale yellow solid. Specifically:

Synthesis of complex 1: Complex **B** (30 mg, 0.048 mmol) and 3-ethynylpyridine (25 mg, 0.242 mmol) were reacted in THF (5 mL) at 40 ºC during 32 h. (23.7 mg, 72 %). ^{1}H NMR (400 MHz, CD_3CN) δ 8.99 (d, *J* = 5.6 Hz, 1H, H_6), 8.39 (d, *J* = 1.7 Hz, 1H, H_{15}), 8.26-8.20 (m, 2H, H_4 + H_{11}), 7.93 – 7.89 (dt_{ap}, *J* = 8.0, 1.6 Hz, 1H, H_{13}), 7.89 (d, *J* = 2.2 Hz, 1H, H_9/H_8), 7.85 (dm, *J* = 8.4 Hz, 1H, H_3), 7.52 (ddd, *J* = 7.5, 5.6, 1.1 Hz, 1H, H_5), 7.39 (d, *J* = 2.2 Hz, 1H, H_9/H_8), 7.29 (ddd, *J* = 8.0, 5.7, 0.6 Hz, 1H, H_{12}), 4.10 (s, 3H, H_{10}), 3.70 (s, 1H, H_{17}). ^{13}C NMR (101 MHz, CD_3CN) δ 197.6 (s, CO), 191.3 (s, CO), 190.3 (s, C_7), 157.1 (s, C_{15}), 154.8 (s, C_{11}), 154.7 (s, C_6), 154.6 (s, C_2), 144.1 (s, C_4), 143.0 (s, C_{13}), 127.3 (s, C_{12}), 126.7 (s, C_9), 125.8 (s, C_5), 123.0 (s, C_{14}), 119.0 (s, C_8), 114.5 (s, C_{13}), 84.8 (s, C_{17}, (*C*C-H)), 78.0 (s, C_{16}, (*C*C-H)), 39.9 (s, C_{10}). HRMS (m/z): 533.0620 [M-OTf], $C_{19}H_{14}AuN_4O_3Re$ (533.0618). IR (cm^{-1}): υ 3238 (CC-H), υ 3238 (C_{Ar}-H), υ 2113 (C≡C), υ 2022, 1926, 1895 (CO), υ 1618 (C_{Ar}=N)

Synthesis of complex 2. 4-ethynylpyridine hydrochloride (85 mg, 0.609 mmol) was dissolved in a saturated aqueous solution of $NaHCO_3$ and extracted with DCM. The organic phase was dried with anhydrous sodium sulfate and the solvent evaporated to dryness to afford 4-ethynylpyridine. Then the alkynylpyridine was reacted with complex **B** following the same procedure described for complex **1** (30 mg, 0.0484 mmol) in THF (5 mL), (29.2 mg, 88 %). ^{1}H NMR (400 MHz, CD_2Cl_2) δ 8.88 (ddd, *J* = 5.6, 1.6, 0.7 Hz, 1H, H_6), 8.26 (ddd, *J* = 8.4, 7.5, 1.7 Hz, 1H, H_4), 8.21 (dd, *J* = 5.1, 1.5 Hz, 2H, H_{11}), 8.19 (d, *J* = 2.2 Hz, 1H, H_9), 8.16 (ddd, *J* = 8.4, 1.7, 1.2 Hz 1H, H_3), 7.50 (ddd, *J* = 7.5, 5.6, 1.2 Hz, 1H, H_5), 7.35 (d, *J* = 2.2 Hz, 1H, H_8), 7.33 (dd, *J* = 5.1, 1.5 Hz, 2H, H_{12}), 4.12 (s, 3H, H_{10}), 3.62 (s, 1H, H_{15}). ^{13}C NMR (101 MHz, CD_2Cl_2) δ 197.4 (s, CO), 197.0 (s, CO), 190.3 (s, CO or C_7), 190.3 (s, CO or C_7), 154.1 (s, C_{12}), 154.1 (s, C_2), 153.8 (s, C_6), 144.1 (s, C_4), 134.2 (s, C_{13}), 129.7 (s, C_{12}), 126.3 (s, C_9), 125.6 (s, C_3), 119.1 (s, C_8), 114.7 (s, C_5), 87.6 (s, C_{15}, (*C*C-H)), 79.5 (s, C_{14}, (*C*C-H)), 39.8 (s, C_{10}). HRMS (m/z): 533.0644 [M-OTf], $C_{19}H_{14}AuN_4O_3Re$ (533.0618). IR (cm^{-1}): υ 3236 (CC-H), υ 3236 (C_{Ar}-H), υ 2117 (C≡C), υ 2019, 1955, 1908 (CO), υ 1620 (C_{Ar}=N)

Synthesis of complex 3. Complex **B** (56.6 mg, 0.091 mmol) and 5-ethynyl-1-methyl-1*H*-imidazole (9.6 µL, 0.091 mmol) were reacted in THF (5 mL) at 40 ºC for 24 h. Purification was carried out by recrystallization in acetone/ether. (23.1 mg, 70 %). ^{1}H NMR (400 MHz, CD_2Cl_2) δ 8.81 (ddd, *J* = 5.6, 1.6, 0.6 Hz, 1H, H_6), 8.20 (ddd, *J* = 8.4, 7.6, 1.6 Hz, 1H, H_4), 8.07 (d, *J* = 2.2 Hz, 1H, H_8), 8.03 (ddd, *J* = 8.4, 1.1, 0.6 Hz, 1H, H_3), 7.42 (ddd, *J* = 7.5, 5.6, 1.1 Hz, 1H, H_5), 7.32 (d, *J* = 2.2 Hz, 1H, H_9), 7.30 (s_{ap}, 1H, H_{16}), 6.96 (d, *J* = 1.3 Hz, 1H, H_{11}), 4.06 (s, 4H, H_{10}), 3.59 (s, 3H, H_{15}), 3.56 (s, 1H, H_{14}). ^{13}C NMR (101 MHz, CD_2Cl_2) δ 197.4 (s, CO), 197.1 (s, CO), 190.8 (s, CO or C_7), 189.7 (s, CO or C_7), 153.9 (s, C_2), 153.5 (s, C_6), 143.4 (s, C_4), 142.6 (s, C_{16}), 136.8 (s, C_{11}), 126.0 (s, C_9), 125.1 (s, C_5), 118.7 (s, C_8), 118.2 (s, C_{12}), 114.4 (s, C_3), 87.2 (s, C_{14}, (*C*C-H)), 69.2 (s, C_{13}, (*C*C-H)), 39.9 (s, C_{10}), 33.6 (s, C_{15}). HRMS (m/z): 536.0738 [M-OTf], $C_{18}H_{15}N_5O_3Re$ (536.0727). IR (cm^{-1}): υ 3229 (CC-H), υ 3129 (C_{Ar}-H), υ 2125 (C≡C), υ 2023, 1945, 1887 (CO), υ 1617 (C_{Ar}=N)

General procedure for gold addition. To a stirred solution of the rhenium precursor (**1**, **2** or **3**) in acetonitrile or dichloromethane (5 mL) was added Au(acac)PPh_3. After 5 hours stirring at r.t. in the dark, the solution was filtered over celite and concentrated to dryness. The solid was redissolved in DCM and addition of ether afforded the desired product as a solid.

Synthesis of complex 4. Complex **4** was obtained following the general procedure for the gold addition. Specifically, compound **1** (58 mg, 0.085 mmol) and Au(acac)PPh_3 (47.5 mg, 0.085 mmol) were stirred in DCM (5 mL) affording the desired product as an orange solid (32.6 mg, 34 %). ^{1}H NMR (400 MHz, CD_2Cl_2) δ 8.89 (dd, *J* = 5.6, 1.6 Hz, 1H, H_6), 8.37 – 8.36 (m, 1H, H_{14}), 8.26 (ddd, *J* = 8.5, 7.6, 1.6 Hz, 1H, H_4), 8.21 (d, *J* = 2.2 Hz, 1H, H_8), 8.17 (d_{br}, *J* = 8.4 Hz, 1H, H_3), 7.87 (dd, *J* = 5.6, 1.4 Hz, 1H, H_{11}), 7.76 (dd, *J* = 8.0, 1.4 Hz, 1H, H_{13}), 7.60 – 7.46 (m, 20H, H_{Ar}+H_5), 7.34 (d, *J* = 2.2 Hz, 1H, H_9), 7.16 (ddd, *J* = 8.0, 5.7, 0.6 Hz, 1H, H_{12}), 4.13 (s, 3H, H_{10}). ^{13}C NMR (101 MHz, CD_2Cl_2) δ 197.6 (s, CO), 197.1 (s, CO), 190.6 (s, C_7), 190.2 (s, CO), 157.0 (s, C_{14}), 154.1 (s, C_2), 153.4 (s, C_6), 150.6 (s, C_{11}), 144.1 (s, C_4), 142.3 (s, C_{13}), 134.8 (d, $^{2}J_{P\text{-}C}$ = 13.8 Hz, 6C, *o*-C, Ph), 132.4 (d, $^{4}J_{P\text{-}C}$ = 2.2 Hz, 3C, *p*-C, Ph), 129.9 (d, $^{1}J_{P\text{-}C}$ = 56.3 Hz, 3C, *i*-C, Ph), 129.9 (d, $^{2}J_{P\text{-}C}$ = 11.4 Hz, 6C, *m*-C, Ph), 126.7 (s, C_{12}), 126.5 (s, C_{15}), 126.2 (s, C_9), 125.51 (s, C_5), 119.2 (s, C_8), 98.0 (brs, C_{16}, (*C*C-H)), 114.7 (s, C_3), 39.8 (s, C_{10}). C_{17} (C*C*-Au) no observed. ^{31}P NMR (162 MHz, CD_3CN) δ 41.49. HRMS (m/z): 991.1122 [M-OTf], $C_{37}H_{28}AuN_4O_3PRe$ (991.1118). IR (cm^{-1}): υ 3124 (C_{Ar}-H), υ 2125 (C≡C), υ 2023, 1900 (CO), υ 1617 (C_{Ar}=N)

Synthesis of complex 5. Complex **5** was obtained following the general procedure for the gold addition. Specifically, compound **2** (30 mg, 0.044 mmol) and Au(acac)PPh_3 (24.6 mg, 0.044 mmol) were stirred in acetonitrile (5 mL) affording the desired product as a red solid (31.2 mg, 62 %). ^{1}H NMR (400 MHz, CD_2Cl_2) δ 8.89 (dd, *J* = 5.6, 0.9 Hz, 1H, H_6), 8.37 – 8.35 (m, 1H, H_{14}), 8.29 – 8.23 (m, 1H, H_4), 8.21 (d, *J* = 2.2 Hz, 1H, H_8), 8.17 (dm, *J* = 8.3 Hz, 1H, H_3), 7.88 – 7.85 (dm, *J* = 5.7 Hz, 1H, H_{11}), 7.76 (dm, *J* = 8.0 Hz, 1H, H_{13}), 7.61 – 7.46 (m, 15H, H_{Ar}), 7.34 (d, *J* = 2.2 Hz, 1H, H_9), 7.17 (ddd, *J* = 8.0, 5.7, 0.7 Hz, 1H, H_{12}), 4.13 (s, 3H, H_{10}). ^{13}C NMR (101 MHz, CD_2Cl_2) δ 197.7 (s, CO), 197.2 (s, CO), 190.6 (s, C_7), 190.5 (s, CO), 154.1 (s, C_6), 153.3 (s, 3C, C_{11}+C_2), 144.0 (s, C_4), 137.5 (s, C_{13}), 134.7 (d, $^{2}J_{P\text{-}C}$ = 13.8 Hz, 6C, *o*-C, Ph), 132.35 (d, $^{4}J_{P\text{-}C}$ = 2.4 Hz, 3C, *p*-C, Ph), 129.8 (d, $^{3}J_{P\text{-}C}$ = 11.4 Hz, 6C, *m*-C, Ph), 129.7 (d, $^{1}J_{P\text{-}C}$ = 56.9 Hz, 3C, *i*-C, Ph), 129.7 (s, 2C, C_{12}), 126.2 (s, C_9), 125.4 (s, C_3), 119.2 (s, C_8), 114.6 (s, C_5), 99.2 (br s, C_{14}, (*C*C-Au)), 39.8 (s, C_{10}). C_{15}(C*C*-Au) no observed. ^{31}P NMR (162 MHz, CD_3CN) δ 41.49. HRMS (m/z): 991.1121 [M-OTf], $C_{37}H_{28}AuN_4O_3PRe$ (991.1118) IR (cm^{-1}): υ 3124 (C_{Ar}-H), υ 2117 (C≡C), υ 2021, 1897 (CO), υ 1602 (C_{Ar}=N).

Synthesis of complex 6. Complex **6** was obtained following the general procedure for the gold addition. Specifically, compound **3** (1 eq, 17.8 mg, 0.026 mmol) and Au(acac)PPh_3 (1 eq, 14.6 mg, 0.026 mmol) were stirred in acetonitrile (5 mL) affording the desired product as a beige solid (16.8 mg, 52 %). ^{1}H NMR (300 MHz, CD_2Cl_2) δ 8.81 (ddd, *J* = 5.6, 1.6, 0.7 Hz, 1H, H_6), 8.20 (ddd, *J* = 8.4, 7.6, 1.7 Hz, 1H, H_4), 8.09 (d, *J* = 2.2 Hz, 1H, H_8), 8.04 (ddd, *J* = 8.4, 1.2, 0.7 Hz, 1H, H_3), 7.60 – 7.45 (m, 16H, H_{Ar}), 7.41 (ddd, *J* = 7.5, 5.6, 1.2 Hz, 1H, H_5), 7.31 (d, *J* = 2.2 Hz, 1H, H_9), 7.15 (d, *J* =1.4 Hz, 1H, H_{11}), 6.59 (d, *J* = 1.4 Hz, 1H, H_{12}), 4.06 (s, 3H, H_{10}), 3.57 (s, 3H, H_{14}). ^{13}C NMR (75 MHz, CD_2Cl_2) δ 197.5 (s, CO), 190.1 (s, CO or C_7), 153.8 (s, C_2), 153.5 (s, C_6), 143.4 (s, C_4), 140.6 (s, C_{11}), 134.74 (d, ^{2}J = 14.4 Hz, 6C, *o*-C, Ph), 133.93 (s, C_{12}), 132.35 (s, *p*-C, Ph), 129.86 (d, $^{1}J_{P\text{-}C}$ = 57.3 Hz, 3C, *i*-C, Ph), 129.73 (d, $^{3}J_{P\text{-}C}$ = 12.0 Hz, 6C, *m*-C, Ph), 125.94 (s, C_9), 125.00 (s, C_5), 120.97 (s, C_{13}), 118.64 (s, C_8), 114.16 (s, C_3), 39.81 (s, C_2), 33.25 (s, C_2). HRMS (m/z): 994.1238 [M-OTf],

$C_{36}H_{29}AuN_5O_3PRe$ (994.1227). IR (cm^{-1}): υ 3127 (C_{Ar}-H), υ 2019, 1893 (CO), υ 1617 (C_{Ar}=N)

ASSOCIATED CONTENT

The Supporting Information is available free of charge on the ACS Publications website.

UV-Vis absorption spectra of **1-6** in DMSO solution ($5 \cdot 10^{-5}$ M), Normalized excitation and emission spectra of complexes **1-6**, imidazolium salt and **A** in DMSO solution at 298 K, Flow cytometry diagram of complex **4** incubated with A549 cell at different concentrations. Incubation of A549 with complex **4** in presence and absence of Z-VAD-fmk, a caspase inhibitor, superposition of UV-Vis absorption graphs of complex **1** (5.10^{-5} M DMSO:PBS, < 0.5 % DMSO) taken over a period of 24 h and superposition of UV-Vis absorption graphs of complex **4** (5.10^{-5} M DMSO:PBS, < 0.5 % DMSO) taken over a period of 24 h.

AUTHOR INFORMATION

Corresponding Author

* vanesa@unizar.es and gimeno@unizar.es

ORCID

Vanesa Fernández-Moreira: 0000-0002-1218-7218
M Concepción Gimeno: 0000-0003-0553-0695

Author contributions

The manuscript was written thought contributions of all authors. All the authors have given approval to the final version of the manuscript.

Notes

the authors declare no competing financial interest.

ACKNOWLEDGMENT

The authors thank the Ministerio de Economía y Competitividad (MINECO-FEDER CTQ2016-75816-C2-1-P and CTQ2015-70371-REDT) and Gobierno de Aragón-Fondo Social Europeo (E07_17R) for financial support. Andrés Luengo thanks Gobierno de Aragón for a predoctoral fellowship.

REFERENCES

(1) Fernández-Moreira, V.; Gimeno M. C. Heterobimetallic Complexes for Theranostic Applications. *Chem. Eur. J.* **2018**, *24*, 3345 – 3353.

(2) Raza, M. K.; Gautam, S.; Garai, A.; Mitra, K.; Kondaiah, P.; Chakravarty, A. R. Monofunctional BODIPY-Appended Imidazoplatin for Cellular Imaging and Mitochondria-Targeted Photocytotoxicity. *Inorg. Chem.* **2017**, *56*, 11019−11029.

(3) Wenzel, M.; de Almeida, A.; Bigaeva, E.; Kavanagh, P.; Picquet, M.; Le Gendre, P.; Bodio, E.; Casini, A. New Luminescent Polynuclear Metal Complexes with Anticancer Properties: Toward Structure–Activity Relationships. *Inorg. Chem.* **2016**, *55*, 2544−2557.

(4) Tasan, S.; Zava, O.; Bertrand, B.; Bernhard, C.; Goze, C.; Picquet, M.; Le Gendre, P.; Harvey, P.; Denat, F.; Casini, A.; Bodio, E. BODIPY–Phosphane as a Versatile Tool for Easy Access to New Metal-Based Theranostics. *Dalton Trans.* **2013**, *42*, 6102−6109.

(5) (a) Lo, K.K.-W.; Zhang, K. Y.; Li, S. P.-Y. Recent Exploitation of Luminescent Rhenium(I) Tricarbonyl Polypyridine Complexes as Biomolecular and Cellular Probes. *Eur. J. Inorg. Chem.* **2011**, 3551–3568; (b) Lo K. K.-W. Luminescent Rhenium(I) and Iridium(III) Polypyridine Complexes as Biological Probes, Imaging Reagents, and Photocytotoxic Agents. *Acc. Chem. Res.* **2015**, *48*, 2985−2995.

(6) (a) Thorp-Greenwood, F. L.; Platts, J. A.; Coogan, M. P. Experimental and Theoretical Characterisation of Phosphorescence from Rhenium Polypyridyl Tricarbonyl Complexes. *Polyhedron* **2014**, 67, 505–512; (b) Kurma, A.; Sun, S.-S.; Lees, A. J. Photophysics and Photochemistry of Organometallic Rhenium Diimine Complexes. *Top Organomet. Chem.* **2010**, 29−35; (c) Lees, A. J. Luminescence Properties of Organometallic Complexes. *Chem, Rev.* **1987**, *87*, 711-743

(7) (a) Fernández-Moreira, V.; Marzo, I.; Gimeno, M. C. Luminescent Re(I) and Re(I)/Au(I) Complexes as Cooperative Partners in Cell Imaging and Cancer Therapy. *Chem. Sci*. **2014**, *5*, 4434−4446; (b) Luengo, A.; Fernández-Moreira, V.; Marzo, I.; Gimeno, M. C. Trackable Metallodrugs Combining Luminescent Re(I) and Bioactive Au(I) Fragments. *Inorg. Chem.* **2017**, *56*, 15159−15170.

(8) Simpson, V.; Casari, I.; Paternoster, S.; Skelton, B. W.; Falasca, M.; Massi, M. Defining the Anti- Cancer Activity of Tricarbonyl Rhenium Complexes: Induction of G2/M Cell Cycle Arrest and Blockade of Aurora- A Kinase Phosphorylation. *Chem. Eur. J.* **2017**, 23, 6518–6521.

(9) Siegmund, D.; Lorenz, N.; Gothe, Y.; Spies, C.; Geissler, B.; Prochnow, P.; Nuernberger, P.; Bandow J. E.; Metzler-Nolte, N. Benzannulated Re(I)–NHC Complexes: Synthesis, Photophysical Properties and Antimicrobial Activity. *Dalton Trans.* **2017**, 46, 15269–15279.

(10) (a) Jin, T.; He, D.; Li, W. Stanton III, C. J.; Pantovich, S. A.; Majetich, G. F.; Schaefer III, H. F.; Agarwal, J.; Wang, D.; Li G. CO2 Reduction with Re(I)–NHC Compounds: Driving Selective Catalysis with a Silicon Nanowire Photoelectrode. *Chem Commun.* **2016**, *52* 14258−14261; (b) Huckaba, J.; Sharpe, E. A.; Delcamp J. H. Photocatalytic Reduction of CO2 with Re-Pyridyl-NHCs. *Inorg. Chem.* **2016**, *55*, 682-690; (c) Ng, C.-O.; Cheng, S.-C.; Chu, W.-K.; Tang, K.-M.; Yiu, S.-M.; Ko, C.-C. Luminescent Rhenium(I) Pyridyldiaminocarbene Complexes: Photophysics, Anion-Binding, and CO2-Capturing Properties. *Inorg. Chem.* **2016**, *55*, 7969−7979; (d) Wang, G.-F.; Liu, Y.-Z.; Chen, X.-T.; Zheng, Y.-X.; Xue, Z.-L. Synthesis, Structure and Luminescent Properties of Rhenium(I) Carbonyl Complexes Containing Pyrimidine-Functionalized *N*-Heterocyclic Carbenes. *Inorg. Chim. Acta* **2013**, *394*, 488−493.

(11) (a) Vaughan, J. G.; Reid, B. L.; Ramchandani, S.; Wright, P. J.; Muzzioli, S.; Skelton, B. W.; Raiteri, P.; Brown, D. H.; Stagni, S.; Massi, M. The Photochemistry of Rhenium(I) Tricarbonyl *N*-Heterocyclic Carbene Complexes. *Dalton Trans.* **2013**, *42*, 14100−14114; (b) Chan, C. Y.; Pellegrini, P. A.; Greguric, I.; Barnard P. J. Rhenium and Technetium Tricarbonyl Complexes of *N*-Heterocyclic Carbene Ligands. *Inorg. Chem.* **2014**, 53, 10862−10873; (c) Mukuta, T.; Simpson; P. V.; Vaughan, J. G.; Skelton, B. W.; Stagni, S.; Massi, M.; Koike, K.; Ishitani, O.; Onda K. Photochemical Processes in a Rhenium(I) Tricarbonyl *N*-Heterocyclic Carbene Complex Studied by Time-Resolved Measurements. *Inorg. Chem.* **2017**, *56*, 3404−3413.

(12) (a) Raba, A.; Anneser, M. R.; Jantke, D.; Cokoja, M.; Hermann, W. A.; Kühn, F. E.; Facile and Scalable Preparation of 2-Imidazolylpyridines. *Tetrahedron Lett.* **2013**, *54*, 3384−3387; (b) Zhuang, R.-T.; Lin, W.-J.; Zhuang, R. R.; Hwang, W.-S. Hg(II), Ag(I) and Au(I) Complexes With Aniline or Pyridine-Functionalized *N*-Heterocyclic Carbene. *Polyhedron*, **2013**, *51*, 132−141.

(13) Casson, A.; Muzzioli, S.; Raiteri, P.; Skelton, B. W.; Stagni, S.; Massi, M.; Brown, D. H. *N*-Heterocyclic Carbenes as π*-Acceptors in Luminescent Re(I) Triscarbonyl Complexes. *Dalton Trans.* **2011**, *40*, 11960−11967.

(14) Stanton, C. J.; Machan, C. W.; Vandezande, J. E.; Jin, T.; Majetich, G. F.; Schaefer, H. F.; Kubiak, C. P.; Li, G.; Agarwal, J. Re(I) NHC Complexes for Electrocatalytic Conversion of CO2. *Inorg Chem.* **2016**, *55*, 3136−3144.

(15) (a) Simpson, P. V.; Skelton, B. W.; Raiteri, P.; Massi, M. Photophysical and Photochemical Studies of Tricarbonyl Rhenium(I) *N*-Heterocyclic Carbene Complexes Containing Azide and Triazolate

Ligands. *New J. Chem.* **2016**, *40*, 5797−5807; (b) Vaughan, J. G.; Reid, B. L.; Wright, P. J.; Ramchandani, S.; Skelton, B. W.; Raiteri, P.; Muzzioli, S.; Brown, D. H.; Stagni, S.; Massi, M. Photophysical and Photochemical Trends in Tricarbonyl Rhenium(I) *N*-Heterocyclic Carbene Complexes. *Inorg. Chem.* **2014**, *53*, 3629−3641.

(16) Li, X.-W.; Li, H.-Y.; Wang, G.-F.; Chen, F.; Li, Y.-Z.; Chen, X.-T.; Zheng, Y.-X.; Xue Z.-L. Blue-Green Luminescent Rhenium(I) Tricarbonyl Complexes with Pyridine-Functionalized *N*-Heterocyclic Carbene Ligands. *Organometallics* **2012**, *31*, 3829−3835.

(17) Fernández-Moreira, V.; Sastre-Martín, H. Photophysical and Bioactivity Behavior of *Fac*-Rhenium(I) Derivatives Containing Ditopic Sulfurpyridine Ligands. *Inorg. Chim. Acta* **2017**, *460*, 127–133.

(18) Casula, A.; Nairi, V.; Fernández-Moreira, V.; Laguna, A.; Lippolis, V.; Garau, A.; Gimeno, M. C. Re(I) Derivatives Functionalised with Thioether Crowns Containing the 1,10-Phenanthroline Subunit as a New Class of Chemosensors. *Dalton Trans.* **2015**, *44*, 18506−18517.

(19) Sacksteder, L. A.; Zipp, A. P.; Brown, E. A.; Streich, J.; Demas, J. N.; DeGraff, B. Luminescence Studies of Pyridine .Alpha.-Diimine Rhenium(I) Tricarbonyl Complexes. *Inorg. Chem.* **1990**, *29*, 4335–4340.

(20) Cunniff, B.; Snider, G. W.; Fredette, N.; Hondal, R. J.; Heintz N. H. A Direct and Continuous Assay for the Determination of Thioredoxin Reductase Activity in Cell Lysates. *Anal. Biochem.* **2013**, *443*, 34−40.

(21) (a) Fernández-Moreira, V.; Ortego, M. L.; Williams, C. F.; Coogan, M. P.; Villacampa, M. D.; Gimeno, M. C. Bioconjugated Rhenium(I) Complexes with Amino Acid Derivatives: Synthesis, Photophysical Properties, and Cell Imaging Studies. *Organometallics* **2012**, *31*, 5950−5957; (b) Wedding, J. L.; Harris, H. H.; Bader, C. A.; Plush, S. E.; Mak, R.; Massi, M.; Brooks, D. A.; Lai, B.; Vogt, S.; Werrett, M. V.; Simpson, P. V.; Skelton B. W.; Stagni, S. Intracellular Distribution and Stability of a Luminescent Rhenium(I) Tricarbonyl Tetrazolato Complex Using Epifluorescence Microscopy in Conjunction with X-Ray Fluorescence Imaging. *Metallomics* **2017**, *9*, 382−390; (c) Balasingham, R. G.; Thorp-Greenwood, F. L.; Williams, C. F.; Coogan, M. P.; Pope, S. J. A. Biologically Compatible, Phosphorescent Dimetallic Rhenium Complexes Linked through Functionalized Alkyl Chains: Syntheses, Spectroscopic Properties, and Applications in Imaging Microscopy. *Inorg. Chem.* **2012**, *51*, 1419−1426.

(22) Sheldrick, G. M. "Crystal structure refinement with SHELXL", *Acta Cryst.* **2015**, *C71*, 3-8.

(23) Ruiz-Leal, M.; George, S. An *In Vitro* Procedure for Evaluation of Early Stage Oxidative Stress in an Established Fish Cell Line Applied to Investigation of PHAH and Pesticide Toxicity. *Mar. Environ. Res.* **2004**, *58*, 631–635.

(24) Gibson, D.; Johnson, B. F. G.; Lewis, J. Metal β-Diketone Complexes. Part VI. Some B-Diketone Complexes of Copper(I), Silver(I), and Gold(I). *J. Chem. Soc. A* **1970**, *0*, 367-369.

Insert Table of Contents artwork here